Phase-resolved spectroscopic modelling of a quasi-periodic oscillation in GRS 1915+105

Edward Nathan, Adam Ingram – University of Oxford

Introduction

GRS 1915+105 is a low mass black hole (BH) X-ray binary (XRB), with the BH accreting matter from a companion star.

The X-ray energy spectra observed from XRBs have 3 main components:

- A multi-colour black body spectrum, coming from a geometrically thin, optically thick disc [1].
- A power-law continuum, cut off at some high energy, of photons Compton up-scattered from a hot population of elections close to the central black hole often referred to as the corona [2].
- A relativistically smeared reflection spectrum from coronal photons which are incident onto the disc, containing many features including a very strong iron Kα line at ~6.4 keV [3].

The physical structure of the corona is still debated. A popular model is that the disc is truncated, inside which the accretion flow becomes optically thin but geometrically thick.

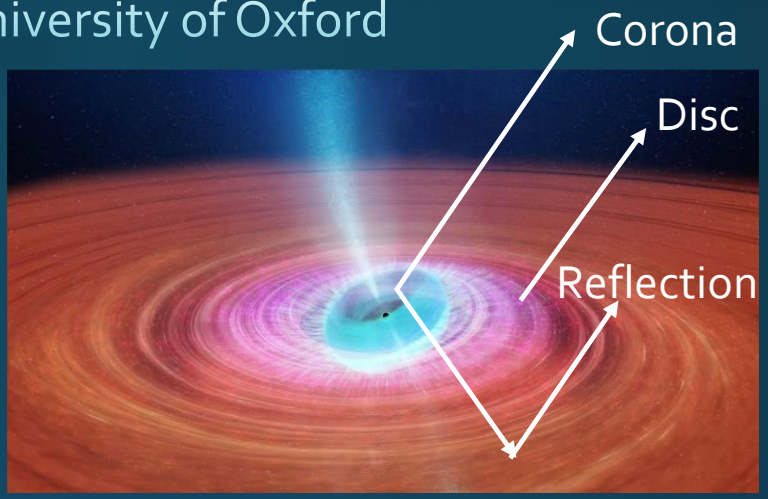

Fig 1: Background still from ICRAR, Miller-Jones et al (2019): https://www.icrar.org/Cygni/ , showing the potentially geometry of a geometrically thin, optically thick disc, which is truncated at some radius, within which a corona is processing. Schematic labels added to show the directly observered corona and disc photons, plus the reflection.

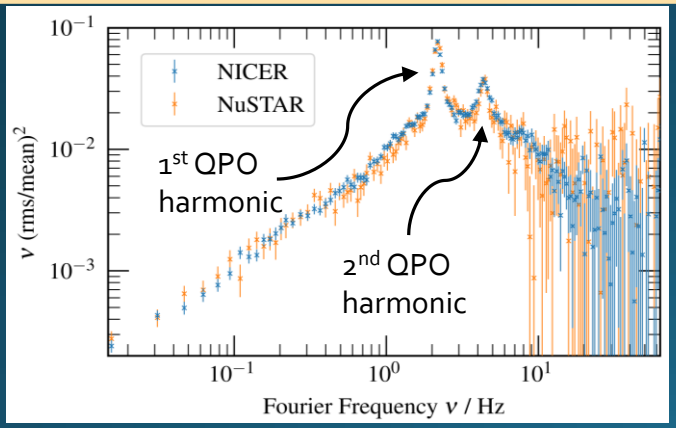

Fig 2: The 3-10~keV power spectra of the *NICER* (blue) and *NuSTAR* (orange) observations, with Poisson noise removed. The power spectra have been ensemble-averaged and geometrically rebinned.

Quasi-periodic Oscillations (QPOs)

QPOs are often seen in the X-ray light curves of XRBs. They appear in the power spectra as peaks which are narrow but have finite width.

The physical mechanism of these has long remained elusive, although it is regularly seen their variability follows the coronal power-law spectrum.

By studying the QPO phase-dependence of the iron Kα line profile in the reflection spectrum, we can test whether the QPO is driven by Lense-Thirring precession of a hot inner accretion flow [4].

We consider a 30 ks joint NICER and NuSTAR observation of GRS 1915+105, which shows a strong 'type-C' low frequency QPO at ~2.2 Hz as can be seen in the 3-10 keV power spectra from each instrument in Fig. 1

Phase-resolved spectroscopy

We want to see how the X-ray spectrum changes with QPO phase. We consider the first two QPO harmonics, in lightcurves from different subject energy bands [5].

In each energy band, we find the **strength** of the two QPO harmonics, and also the **phase-lag** between the QPO harmonics in each energy band compared to their respective harmonics in a *reference energy band*, which taken as the full energy range of each instrument.
Finally, we calculated the **phase difference** between the two QPO harmonics in the reference band.

We put these three pieces of information together, and can construct a second order Fourier series for the QPO, and extract real and imaginary parts of the Fourier transformed (FT) spectra for the first two QPO harmonics.

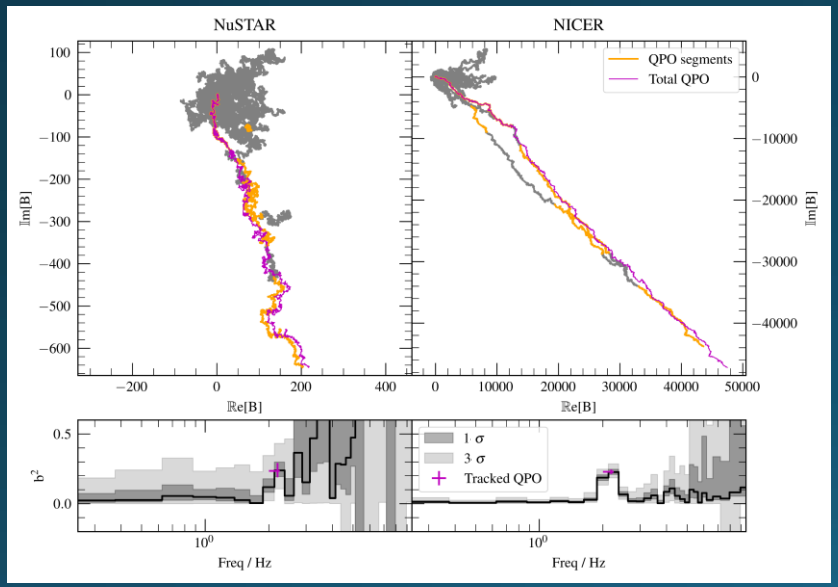

Fig 4: Estimation of the phase difference between the two harmonics in the reference band, for both *NuSTAR* and *NICER*. Calculated using the bi-spectrum, the angle of each path on the relates to the bi-phase (and hence phase difference) between any Fourier frequency and it's double. Beneath this, the bi-coherence of these frequency pairs is shown, along with the 1 and 3 σ confidence levels. The bi-coherence is only significantly non-zero for the QPO fundamental and 2nd harmonic.

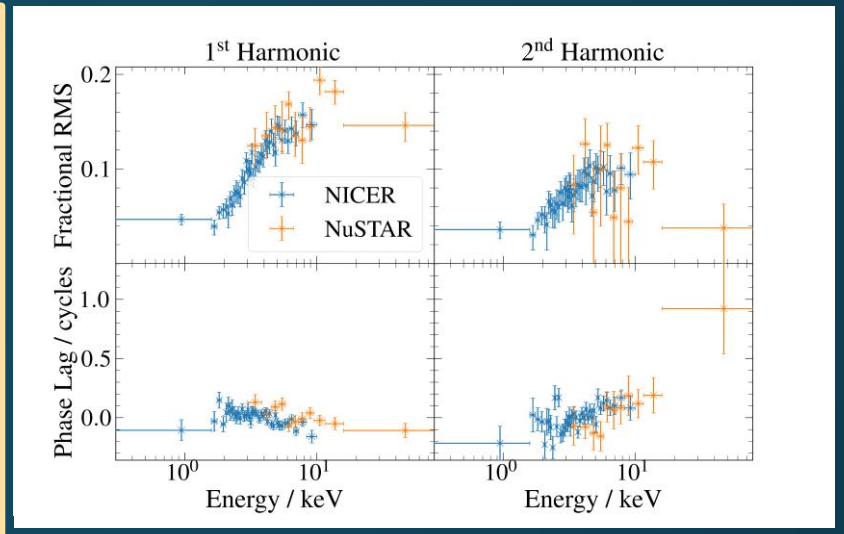

Fig 3: The fractional RMS and phase lags of the first and second harmonics of the QPO in both the *NICER* and *NuSTAR* observations in different energy bands.

QPO Frequency Tracking

Our simultaneous *NICER* and *NuSTAR* observations both have ~30 ks of exposure, which was taken over the course of ~62 ks (~17 hours).
Over this time, the QPO frequency drifts. We therefore use a tracking algorithm to find the QPO frequency at any given time, and correct for this drift.

Fig 4: The estimated value of the QPO frequency measured in each 64 s long segment of the two light curves, with the error bars denoting the estimated QPO FWHM. The grey dashed line show the dynamic bounds for the QPO tracking algorithm. The red line is a 15 deg polynomial simultaneously fit to the estimated QPO frequencies, which we then use to get the QPO frequency at arbitrary time.

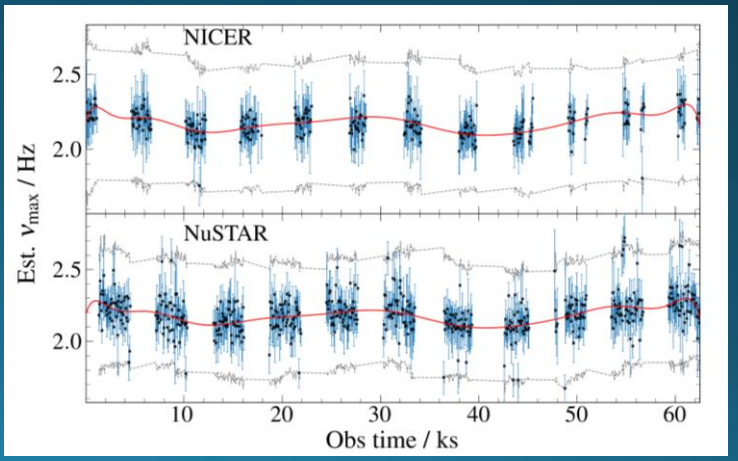

The Model – Overview

We construct a model for the three major components of the energy spectrum, however we allow certain key parameters to be modulated with QPO phase γ, assuming two harmonics [6]. Using the coronal normalisation as an example,

$$N_c(\gamma) = N_c + A_{1N}\sin[\gamma - \phi_{1N}] + A_{2N}\sin\left[\frac{1}{2}(\gamma - \phi_{1N})\right]$$

where N_c is the phase-average value, and $A_{1N}, A_{2N}, \phi_{1N}, \phi_{2N}$ are the amplitudes and phases of the two harmonics.

We evaluate this model for 16 QPO phases, and use a Fourier transform to find the real and imaginary components of the first two QPO harmonics.

The Model - Corona

The only assumption about the corona that we make is that its bolometric luminosity is constant in time, so that variation in the observed flux caused by its motion with respect to our viewing angle over the QPO cycle.

We use the model NTHCOMP – a power-law model with photons/energy $\propto E^{-\Gamma}$ between the seed photon temperature, and the electron temperature kT_e. We also assume some reflection fraction of this flux is illuminating back onto the disc.

We allow the corona's normalisation N_c, the photon index Γ, and the electron temperature kT_e to vary with QPO phase.

The Model - Reflection

We use the XILLVERCP reflection model, which we raytrace to account for relativistic effects and also so we can consider local disc ionisation and illumination.

We assume that a fraction of the coronal photons are incident upon the disc, based upon a QPO phase dependent emissivity profile at disc radial and azimuthal coordinates r and ϕ

$$\epsilon(r,\phi,\gamma) \propto \epsilon(r)\left\{1 + A_1\cos^2\left[\frac{1}{2}(\gamma - \phi + \phi_1)\right] + A_2\cos^2[\gamma - \phi + \phi_2]\right\}$$

where A_1, A_2, ϕ_1, and ϕ_2 are the free *asymmetry* parameters in the model, so that $A_1 = A_2 = 0$ represents an axi-symmetric and QPO phase independent emissivity profile. $\epsilon(r)$ is a twice-broken power-law which we use for the radial dependence.

We also assume a radial ionisation profile, which is modulated in proportion to the modulations in the irradiation flux.

The Model - Disc

We assume simple blackbody emission, which a constant viscous heating temperature, and we also include an additional temperature increase from the irradiating flux. This is also modulated in proportion to the modulations in the irradiating flux, but with a phase-lag to account for a thermalisation time.

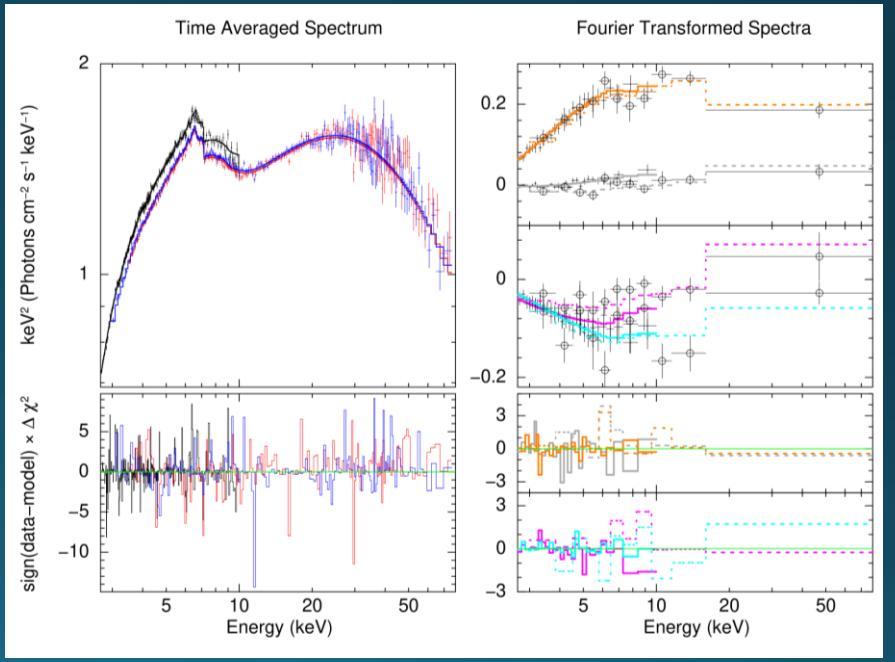

Fig 6: The best fit model for the flux-energy spectra (left) and the harmonics of the QPO (right). The flux-energy spectra from *NICER* is in black, *NuSTAR* FPMA is in red, and *NuSTAR* FPMB is in blue. The spectra of the real and imaginary components of the 1st QPO harmonic are in grey and orange respectively; the 2nd QPO harmonic components are shown in magenta and light blue. Both harmonics have the *NuSTAR* data points with circles and a dotted line, with the circle-less points and solid lines corresponding to *NICER*.

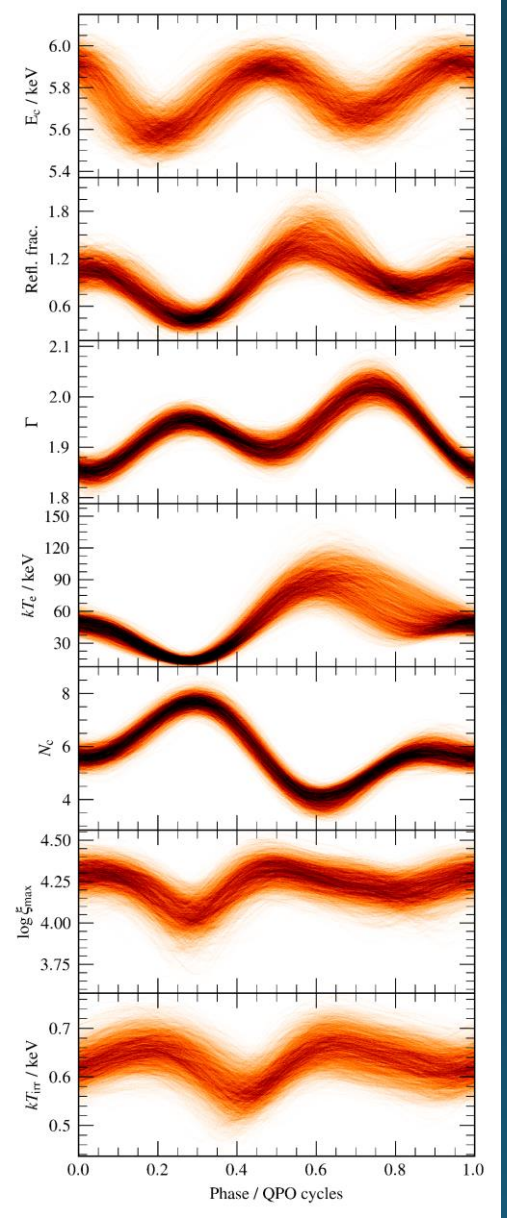

Fig 7: Curves produced from the parameters from steps in the MCMC. The iron-line centroid energy E_c was calculated from the varying illumination profile. The reflection fraction, Γ, kT_e, and N_c are the modulations straight from their parameters in the model, whereas $\log \xi_{max}$ and kT_e are calculated from the irradiating flux.

MCMC and Results

We simultaneously fit our model to the phase-average and phase-resolved spectra from both *NICER* and *NuSTAR*, with the best fit shown in Fig 6.

We use an MCMC to sample the parameter space. For each step in the MCMC, we are able to reconstruct the parameter modulations which we show in Fig 7. In the figure, we also show the centroid energy of the iron Kα which varies due to patches of the disc being preferentially illuminated, which are seen with different blue/redshifts. Finally, we also show the additional disc heating and ionisation, as are calculated as in the model.

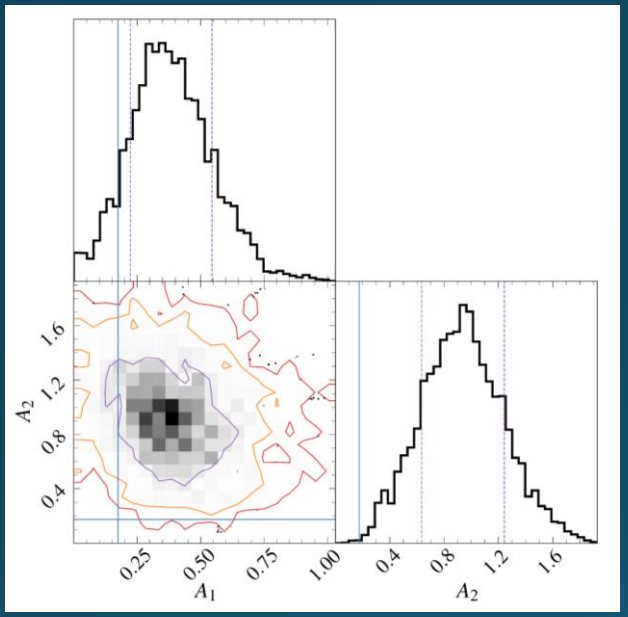

Fig 8: A_1 and A_2 contour based around the MCMC. Contour levels containing 1, 2, and 3 σ of the chain mass are shown (purple, orange, red), with the blue lines highlighting the values at the best-fit. Outside the 3 σ contour individual points are shown as grey points.

Asymmetry Parameters

We show the posterior distribution of the A_1 and A_2 asymmetry parameters in Fig 8, calculated from the MCMC. This shows that the $(0, 0)$ coordinate (which corresponds to the axi-symmetric case) is excluded to a high significance. This adds to the strong evidence that the QPO is caused by a precession model.

However, the same fit also required a very small truncation radius for the disc $r_{in} = 1.43^{+0.01}_{-0.02}\ r_G$, which doesn't leave much room for the corona to process inside this radius. If this is correct, then the asymmetric emissivity profile could be a result of, e.g. the base of a processing jet, or some other geometry.

Contact Information
edward.nathan@physics.ox.ac.uk

References

1. Shakura NI, Sunyaev RA. Black holes in binary systems. Observational appearance. Astronomy and Astrophysics. 1973;24:337-55.
2. Thorne KS, Price RH. Cygnus X-1-an interpretation of the spectrum and its variability. The Astrophysical Journal. 1975 Feb;195:L101-5.
3. George IM, Fabian AC. X-ray reflection from cold matter in active galactic nuclei and X-ray binaries. MNRAS. 1991 Mar 15;249(2):352-67.
4. Ingram A, van der Klis M, Middleton M, Done C, Altamirano D, Heil L, Uttley P, Axelsson M. A quasi-periodic modulation of the iron line centroid energy in the black hole binary H1743−322. MNRAS. 2016 Sep 11;461(2):1967-80.
5. Ingram A, van der Klis M. Phase-resolved spectroscopy of low-frequency quasi-periodic oscillations in GRS 1915+ 105. MNRAS. 2015 Feb 1;446(4):3516-25.
6. Ingram A, van der Klis M, Middleton M, Altamirano D, Uttley P. Tomographic reflection modelling of quasi-periodic oscillations in the black hole binary H 1743− 322. MNRAS. 2017 Jan 1;464(3):2979-91.

Figures 2-8 are from Nathan et al (in prep)